Standalone Interferometry-Based Calibration of Convex Lens-Induced Confinement Microscopy with Nanoscale Accuracy†

Gregory T. Morrin[a], Daniel F. Kienle[a], and Daniel K. Schwartz*[a]

ABSTRACT

Strongly confined environments (confined dimensions between 1-100 nm) represent unique challenges and opportunities for understanding and manipulating molecular behavior due to the significant effects of electric double layers, high surface-area to volume ratios, and other phenomena at the nanoscale. Convex Lens-induced Confinement (CLiC) can be used to analyze the dynamics of individual molecules or particles confined in a planar slit geometry with continuously varying gap thickness. We describe an interferometry-based method for precise measurement of the slit pore geometry. Specifically, this approach permitted accurate characterization of separation distances as small as 5 nm, with 1 nm precision, without a priori knowledge or assumptions about the contact geometry, as well as a greatly simplified experimental setup that required only a lens, coverslip, and inverted microscope. The interferometry-based measurement of gap height offered a distinct advantage over conventional fluorescent dye-based methods; e.g., accurate interferometric height measurements were made at low gap heights regardless of solution conditions, while the concentration of fluorescent dye was significantly impacted by solution conditions such as ionic strength or pH. The accuracy of the interferometric measurements was demonstrated by comparing the experimentally measured

[a] Department of Chemical and Biological Engineering,
University of Colorado Boulder, Boulder, CO, 80309
Email: daniel.schwartz@colorado.edu
† Electronic supplementary information (ESI) available.

concentration of a charged fluorescent dye as a function of gap thickness with dye concentration profiles calculated using Debye-Hückel theory. Accurate characterization of nanoscale gap thickness will enable researchers to study a variety of practical and biologically relevant systems within the CLiC geometry.

TOC Graphic

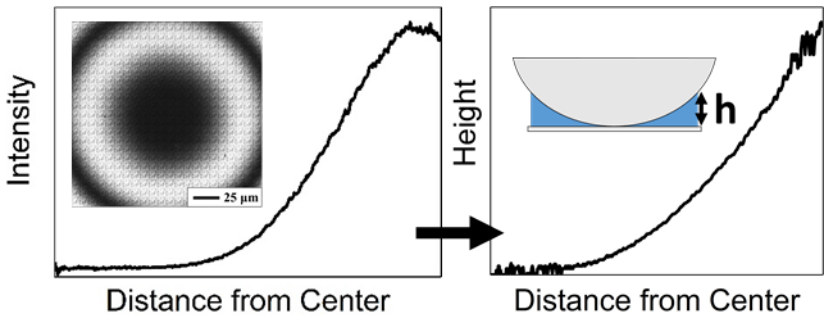
Intensity
25 µm
Distance from Center
Height
h
Distance from Center

INTRODUCTION

Confined nanoscale geometries represent unique environments for studying the dynamics of particles and macromolecules due to the significant effects of electric double layers between charged surfaces, large surface area-to-volume ratios, and characteristic dimensions that are similar in size to a variety of biomolecules and nanoparticles[1–6]. These properties have been leveraged for a number of practical applications; recent advances in bioseparations[7–9], biosensing[10–13], single molecule analysis[14–17], and the understanding of solvent behavior within interface-rich environments[18] have been made possible by studying and manipulating molecular behavior in nano-confinement. Producing and characterizing these highly confined environments in an accessible way remains a key challenge for researchers[19–23].

Convex Lens-induced Confinement (CLiC) has shown significant promise in addressing this challenge. In their seminal publication on the method, Cohen and coworkers[24] showed that a wide range of gap heights (i.e., confined liquid film thickness) from several μm down to the nanoscale could be created by placing a convex lens in contact with a glass coverslip, which was used to study the behavior of molecules in solution. The confinement of individual molecules enabled longer tracking times and the observation of single molecules at higher analyte concentrations (due to the reduced background fluorescence) when compared to other methods such as total internal reflection fluorescence and confocal microscopy, as well as provided an effective nanoslit geometry in which the behavior of particles at various gap heights could be studied[24]. These methods were extended by the Leslie lab, which demonstrated various applications of the CLiC geometry through the determination of free energies of confinement[25], electric-field assisted free energies within confinement[26], and DNA hybridization events (determined using Förster Resonance Energy Transfer or FRET)[27].

Previous CLiC experiments focused mainly on dynamics within environments with characteristic confinement dimensions in the range of several hundred nm to several μm, where the gap thickness was readily characterized with little ambiguity. In experiments that explored smaller gap dimensions, measurements of gap size employed implicit assumptions about solution conditions, which might not be appropriate at low ionic strengths, and a simplified view of the contact mechanics between the lens and coverslip, which could significantly affect the gap profile at small separation distances. While gap heights on the order of a hundred nanometers or higher are relevant to many industrial and biological applications, there are many situations where smaller gap heights are critically important. Many separations techniques, including protein separation using ultrafiltration[28,29], as well as recent analytical methods such as electrochemical correlation spectroscopy[30] occur within environments that have confined dimensions on the order of tens of nanometers. Within the evolving field of nanofluidics, there remain unique challenges as well as opportunities associated with strongly confined molecular transport (confined dimensions between 1-100 nm)[31]. For example, Renaud and co-workers found that protein diffusion within 50 nm channels was significantly impacted by the high surface area-to-volume ratio of the channel, which increased the frequency of reversible surface interactions, and was also impacted by electric double layer effects within the channel, which substantially altered the effective volume available for diffusion[32]. Additionally, theoretical studies where critical polyelectrolyte adsorption within confinement was simulated (using a range of parameters pertinent to applications such as nucleic acid adsorption within viral capsids) were performed at slit heights of approximately 10 nm, where the authors found non-monotonic adsorption behavior as a function of ionic strength due to the interplay of electrostatic forces (enhanced by overlapping electric double layers) and entropic penalties[33]. Here, we present

methods to extend the measurement of the confined CLiC gap thickness down to these smaller nanoscale dimensions in order to more accurately measure molecular and particle dynamics at the sub-100 nm scale.

Here, we enhanced the capabilities of the CLiC method by accurately characterizing gap heights down to 5 nm using an interferometric method that was not influenced by variations in ionic strength and did not require the addition of other reagents, such as fluorescent dye. Moreover, this allowed us to implement a simple and experimentally accessible realization of the CLiC geometry, which did not require the use of counterweighted lens holders or additional mechanical fixtures. In order to validate the accuracy of the interferometrically measured height profile, experimental measurements of fluorescent dye concentration profiles (vs. gap height) were made at various values of ionic strength and compared to theoretical predictions based on the Poisson-Boltzmann equation.

EXPERIMENTAL

Imaging System & Lens/Coverslip Setup

Two lasers were used for the experiments: a 488 nm wavelength Ar-ion laser (Melles Griot) was used for interferometry measurements and a 561 nm wavelength laser (Coherent) was used to excite fluorescent dye. Details about the imaging system setup are described on page S-2 of the Electronic Supporting Information (ESI). The experimental setup for the lens and coverslip was the same for both interferometric gap height characterization and fluorescent dye images. Specifically, approximately 35 uL of solution was pipetted onto a clean coverslip resting on the microscope stage, and a lens was carefully placed immediately onto the liquid on the

coverslip, convex side down, using tweezers. A description of the cleaning process used for the lens and coverslip can be found on page S-3 of the ESI.

Interferometry-Based Height Profile Measurement

Interference patterns were analyzed using custom Matlab software. A full description of the image analysis and height determination is provided on pages S-4 through S-7 of the ESI. Briefly, the center of the contact region of the interference pattern was determined by finding the centroid of the first interference ring. Radially averaged intensities were then calculated as a function of distance from the center, which were used as inputs for the height calculations. The heights were determined numerically using a multilayer-matrix method[34] which describes the propagation of light through stratified media using optical transfer matrices. Specifically, the theoretical transmissivity was calculated as a function of the gap height using a previously described software algorithm[35]. The theoretical and experimentally measured (radially averaged) intensities were rescaled such that a value of 0 represented the intensity in the contact patch, and a value of 1 represented the intensity of the first interference peak (determined for experimental data as the maximum of the intensity data, smoothed using a Savitzky-Golay filter). The gap height was then computationally determined as the height that minimized the difference between the theoretical and experimental transmissivities (for a complete description, please see the ESI).

Measurement of the Height Profile Using Fluorescent Dyes

Alexa Fluor 555 dye (Invitrogen, Cat No. 20009) was added at a concentration of 8 μM to aqueous solutions of varying ionic strength that were prepared using sodium chloride (Acros Organics) dissolved in ultrapure water. Images of the bulk dye solution within the CLiC geometry were analyzed in Matlab. In order to calculate height profiles from dye images, dye

intensities were converted to height using a proportionality constant based on the intensity of the dye at the radial location of the first interference fringe, where the gap height was known accurately (see ESI **Table S-1** for proportionality constant values).

Dye Concentration Profile Measurement

Experimental measurements of dye concentration as a function of height were obtained from images of the dye solution within the CLiC geometry. For a detailed description of the analysis, see pages S-9 through S-11 of the ESI. Briefly, the center of the contact region in the dye image was determined by fitting the intensity values within the image to a second order two-dimensional polynomial, and radially averaged intensities were then calculated as a function of distance from the center of the contact region. Dye intensity profiles were then converted to concentration using a proportionality constant that was found by fitting the intensity profile at gap sizes with fully developed electrical double layers (defined as heights greater than six Debye lengths).

RESULTS & DISCUSSION

Interferometric Height Profile Measurement

The height profile of the lens as a function of distance from the center of the contact region is shown in **Figure 1**. We assume that the initial, relatively noisy region near the center of the contact region corresponded to the upper bound of the radius of contact between the lens and the coverslip. Since both the lens and coverslip were considered linear elastic materials (fused silica and borosilicate glass, respectively) they were expected to deform when the lens was placed on the coverslip due to the applied load. This produced a circular region of contact whose dimensions could be theoretically calculated and compared to experimental

measurements; in our case, Hertzian assumptions were made in order to estimate the contact region since the surfaces were not molecularly smooth and had some degree of roughness[36]. At the Hertzian limit, the radius of the contact region could be determined using the relationship[36]:

$$a = \sqrt[3]{\frac{3FR}{4E^*}} \quad (1)$$

Where *a* represented the radius of the contact region, *F* represented the loading force, *R* represented the radius of the lens, and *E** represented the reduced modulus of the glass surfaces. Parameters that were used for the equation are described on page S-12 of the ESI. The theoretical contact region radius, *a*, was approximately 15 μm, which was in reasonable agreement with the measured radius of the contact region. The contribution of coverslip flexure to the contact region did not appear to have a significant effect on the contact radius, as evidenced by the good agreement of the measured contact radius and theoretical Hertzian contact radius (which assumes an elastic half-space). Outside of the contact region, height measurements down to approximately 5 nm were determined to have uncertainties of approximately 1 nm, as indicated by the confidence intervals on the height profile. We noted that there was a significantly higher degree of noise within the profile at heights that corresponded to the first interference fringe (approximately 92 nm) when compared to the rest of the height profile. This was due to the fact that the variation of height with intensity followed an inverse cosine function [37], which has its steepest slopes at the peak and trough of the interference fringes, such that small fluctuations in the intensity caused large errors in the height calculation.

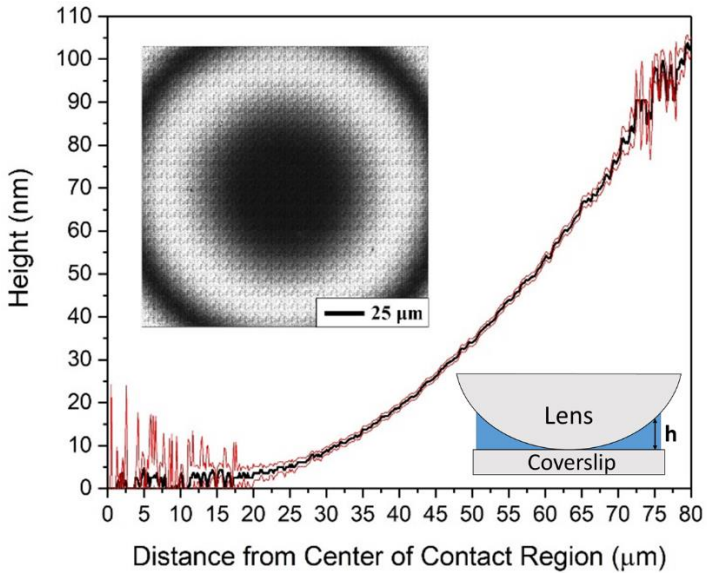

Figure 1. Height profile of the gap between lens and coverslip as a function of distance from the center of the contact region (black line). Red lines represent 95% confidence intervals. Inset, upper left: Multiple field-of-view interference pattern used to determine the height profile. Inset, lower right: diagram illustrating the CLiC geometry.

Interferometric Height Comparison with Dye Height Profile Measurements

While interferometry-based measurements of the height profile were previously used for gap heights greater than or equal to the height corresponding to the first interference fringe (due to the formation of Newton's rings[38]), they were not employed to measure smaller CLiC gap heights. In fact, the most common approach to measure the height for these smaller gap thicknesses (i.e. smaller than the thickness associated with the first interference fringe) required the penetration of fluorescent dye into the gap, where emission intensity was measured as a function of radial position[24,25,39–41]. This method was most accurate in the limit where dye molecules had negligible interactions with the confining surfaces (such as electrostatic interactions) as well as minimal adsorption at these interfaces. Assuming these criteria were met, the intensity at a given pixel would be proportional to the height at that point[24]. However, ionic

strength could significantly affect the electrostatic interactions between dyes and the surfaces confining them, particularly when the gap height was on the order of the Debye length in solution [42]. Moreover, surface adsorption could also potentially skew such interpretations. We measured the intensity of a negatively charged fluorescent dye molecule within the gap between the lens and coverslip (both of which were also negatively charged) under conditions where a significant degree of electrostatic dye exclusion was observed. As shown in **Figure 2A-C**, the penetration of dye molecules near the lens/coverslip contact region was significantly affected by electrostatic effects—as shown by the shrinking of the dark excluded region—as the electrostatic repulsion between the surface and the dye molecules was increasingly screened by higher concentrations of sodium counter-ions. These qualitative differences were reflected in the apparent height profiles calculated from the intensity measurements (see **Figure 2D**). Clearly, the apparent height profiles measured using dye intensities required significant corrections in order to account for the repulsive interactions that reduced dye concentration at these small gap heights.

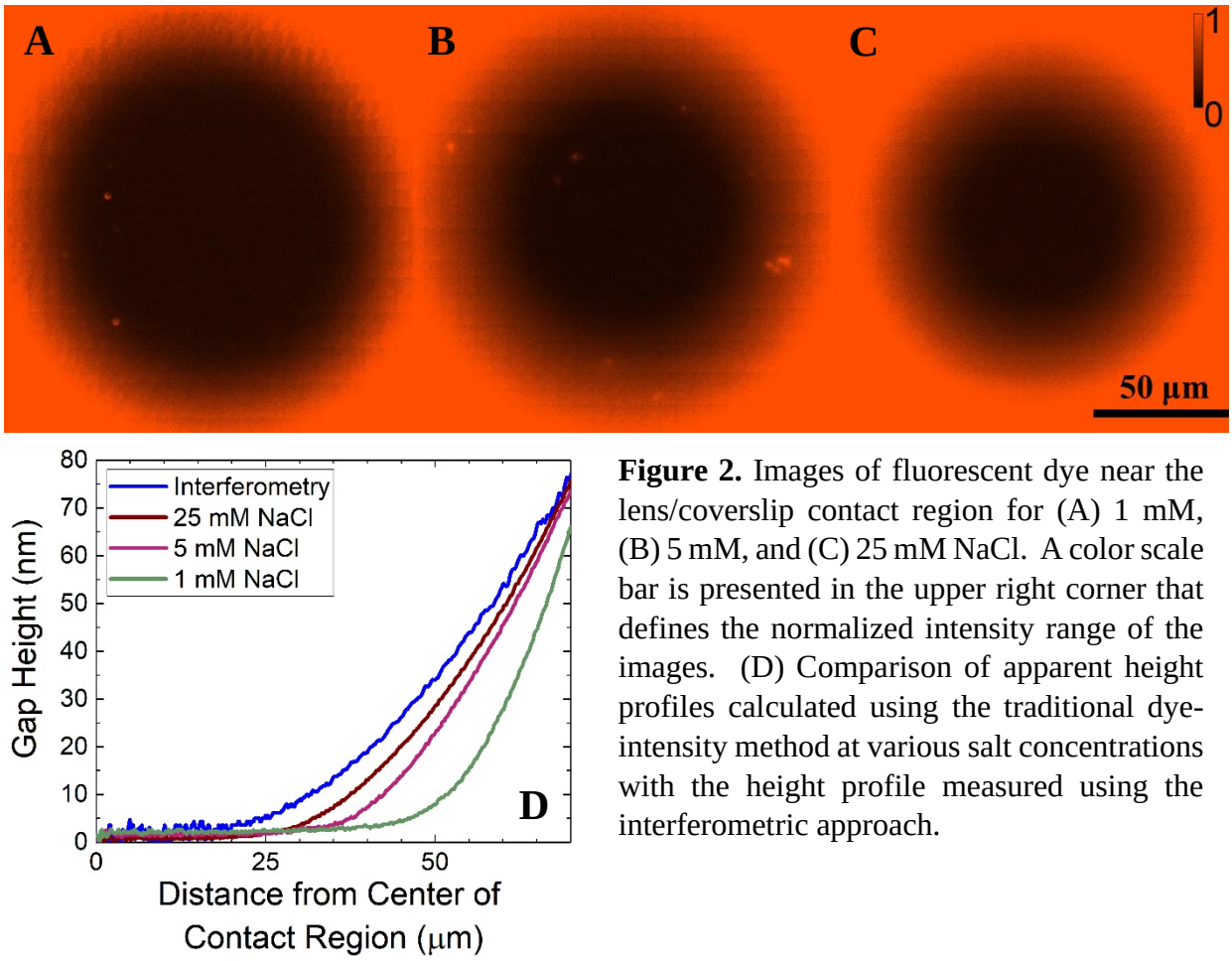

Figure 2. Images of fluorescent dye near the lens/coverslip contact region for (A) 1 mM, (B) 5 mM, and (C) 25 mM NaCl. A color scale bar is presented in the upper right corner that defines the normalized intensity range of the images. (D) Comparison of apparent height profiles calculated using the traditional dye-intensity method at various salt concentrations with the height profile measured using the interferometric approach.

As the salt concentration was increased the profiles systematically approached the interferometric profile, consistent with expectations as the electrostatic repulsion of dye molecules was increasingly screened, which permitted better penetration of the dye, and resulted in improved height characterization. However, this limited the utility of dye-intensity gap thickness characterization to high ionic strength conditions. Moreover, as the ionic strength was increased, it was common to observe additional intensity artifacts due to increased surface adsorption.

Experimental Measurement Comparison with Theoretical Predictions

In order to validate the accuracy of the interferometry-based height measurements, the concentration of dye as a function of height was experimentally determined and compared to theoretical predictions based on the Poisson-Boltzmann equation. The theoretical model was based on the work done by Renaud and co-workers studying dye diffusion in glass nanochannels[6,42], where a Boltzmann distribution was used to describe the equilibrium concentration of various ions in solution as a function of electric potential (assumed to vary only in the direction normal to the glass surfaces):

$$C_i(z) = C_{B,i} \exp[-\frac{q * \psi(z)}{k_B T}] \quad (2)$$

Where C_i represented the concentration of a particular ion at a distance z from the surface, $C_{B,I}$ represented the bulk concentration of the ion, q represented the charge of the ion, $\psi(z)$ represented the electric potential at a distance z from the surface, k_B represented the Boltzmann constant, and T represented the temperature. The expression for the electric potential was derived using the Debye-Hückel approximation[6], a linearized form of the Poisson-Boltzmann equation appropriate under these conditions, which leads to the following analytical expression:

$$\psi(z) = \frac{\zeta \cosh\left[\left(\frac{h}{2} - z\right)/\lambda_D\right]}{\cosh\left(\frac{h}{2\lambda_D}\right)} \quad (3)$$

where ζ represented the zeta potential of the surface, h represented the gap height, z represented the distance from the surface, and λ_D represented the Debye length of the solution. The parameters used to calculate the electric potential, such as the zeta potential and Debye length, are described on pages S-13 and S-14 of the ESI. The average predicted concentration of dye for

a given gap height was calculated by integrating the theoretical concentration over the entire height of the slit, and dividing by the slit height.

In order to compare the theoretical calculations directly to experimental data, measurements of the intensity as a function of height were converted to concentration (see pages S-9 through S-11 of the ESI). Comparisons between theoretical calculations and experimental results are shown in **Figure 3**. Overall, good agreement was found between the experimental data and theoretical predictions, confirming that the height measurements from the interferometry-based approach were accurate. Importantly, the concentration of dye at all levels of ionic strength tested were significantly different from the bulk concentration over a large range of heights at the nanoscale. Within this region, the penetration of dye was strongly impacted by electrostatic forces, illustrating both the unique phenomena that occur at this length scale as well as the need for a method that could measure gap heights without being affected by solution conditions such as ionic strength.

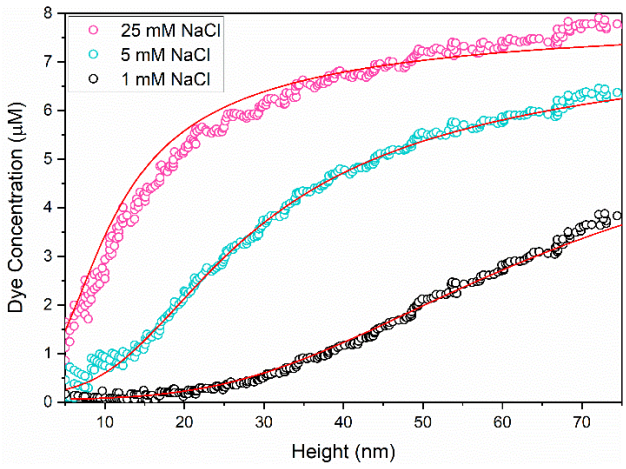

Figure 3. Dye concentration plotted as a function of gap height for various salt concentrations. Experimental measurements are represented by open circles (○) and theoretical predictions are represented by red lines. Confidence intervals were smaller than the symbols representing the experimental data. Data was cut off at 5 nm due to greater uncertainty at low intensities.

CLiC Method Comparison and Current System Limitations

Previous measurements of very small gap heights in CLiC systems did not explicitly account for contact mechanics between the glass coverslip and lens, which lead to a contact area ("patch") as opposed to a single point of contact, as frequently assumed. Assumptions related to the contact mechanics between the lens and coverslip can have a significant effect on the calculated height profile below the first interference fringe. In previous studies, dye intensity measurements used to determine the height profile included the entire region around the contact point and assumed non-zero height, rather than accounting for a contact region using a constant average intensity and zero gap height. As described above, we found that deformations due to contact mechanics had a particularly large influence in the small gap thickness regime. Even if counterweights were used to reduce the load due to the effective weight of the lens, a significant contact region is expected to form due to the residual weight, in addition to other attractive forces including capillary interactions and van der Waals forces. For example, if a counterweight was used to offset approximately 90% of the weight of the lens, as in previous work[24], this would still result in a contact region with a radius of at least 7 μm, assuming common literature values for the elastic moduli and Poisson ratios of the coverslip and lens, but ignoring additional loading due to other attractive interactions. While the effect of the contact region becomes unimportant at large radial distances, where the gap height is large, it significantly influences the accuracy of the profile in the small gap thickness regime. This may explain apparent discrepancies previously reported between the actual molecular dimensions and those inferred from dye intensity measurements, where molecular diameters inferred from exclusion at small gap height consistently overestimated their known sizes[24]. Notably, some recent CLiC implementations attempted to account for contact area phenomena[40]. Experiments

that focus on phenomena involving nanoscale gaps will benefit greatly from an accurate and independent measurement of gap thickness, that does not require ad hoc assumptions about dye penetration.

The methods reported here provided significantly improved accuracy of CLiC height profiles, particularly in the nanoscale regime. CLiC has been effectively leveraged for single molecule studies that investigated the effects of confinement on relatively large molecules at scales ranging between about a hundred nanometers to several microns. By improving height profile measurements below the first interference fringe, confined dimensions relevant to smaller molecules can now also be performed with better precision using CLiC. Moreover, this approach enabled a greatly simplified experimental setup, that did not require complex or custom mechanical components, such as frictionless counterweights. Here, we demonstrated that experiments could readily probe the behavior of molecules with nanoscale gaps using only a lens, coverslip, and a conventional inverted microscope. By eliminating the need for free dye in solution for height estimation, potentially unwanted interactions between the fluorescent probe and the analyte of interest were avoided and the range of wavelengths available for probe excitation was expanded (a useful feature for experiments where multiple dyes may be required, such as FRET). In future studies, the interferometric approach will allow a broader range of systems to be studied with *in situ* measurements of the height profile. Additionally, by using the multilayer-matrix-method, extension to confining surfaces modified with additional independently characterized films will be possible.

We also note some limitations to our approach; if flow is required or solution exchange is needed, the current experimental setup may not be sufficient, and previous CLiC implementations should be considered[27,39,40,43]. It is worth noting that hybrid approaches can

also be performed, where an interferometry-based approach for height measurements near the contact region can be combined with a complex, high-throughput CLiC system. For CLiC experiments where patterned surfaces may be necessary[41], an interferometric approach may be difficult to implement. However, there have been a number of experiments where the CLiC geometry alone provided a suitable environment for studying the dynamics of large molecules as a function of confinement[24,25,44]. An extension of these types of experiments to smaller gap thickness will enable the study of molecular behavior at varying degrees of confinement that are relevant to a wide range of applications, including protein separation methods[28,29], polyelectrolyte adsorption at biointerfaces[45], and single-molecule sensors[46].

CONCLUSIONS

An accurate method for measuring confined molecular dynamics at the nanoscale was developed based on confinement between a convex lens and a planar fused silica wafer. The accuracy of the method was validated through the agreement of experimental results with predictions from the linearized Poisson-Boltzmann equation, where negatively charged dye molecules were increasingly excluded from negatively charged gaps as the ionic strength was decreased. Using interferometry, rather than free fluorescent dyes in solution, gap heights as small as 5 nm were consistently measured with nm precision, regardless of the strength of interactions (e.g. electrostatic forces, surface affinity) within the confined environment, extending the range of heights that can be used to study single-molecule behavior in confinement. Another key advantage of the system was its experimental simplicity. The method described here will provide an easily accessible nanoscale system for researchers studying confined molecular dynamics.

CONFLICTS OF INTEREST

There are no conflicts to declare.

ACKNOWLEDGEMENTS

The authors would like to thank Raphael Sarfati for useful discussions pertaining to the analyses. G.T.M. and D.K.S. were supported by the U.S. Department of Energy, Office of Science, Basic Energy Sciences (award #DE-SC0001854) for data acquisition, statistical analysis, interpretation of the results, and manuscript preparation. Additional support for G.T.M.'s graduate training was provided by the NIH/CU Molecular Biophysics Graduate Traineeship T32 GM065103. Support for D.F.K. was provided by the U.S. Defense Threat Reduction Agency (award #HDTRA1-16-1-0045) for development of data analysis methods. The imaging work was performed at the BioFrontiers Institute Advanced Light Microscopy Core. TIRF microscopy was performed on a Nikon A1R microscope supported by NIST-CU Cooperative Agreement (award #70NANB15H226). ***REFERENCES***

1 A. Piruska, M. Gong, J. V Sweedler and P. W. Bohn, *Chem. Soc. Rev.*, 2009, **39**, 1060–1072.

2 M. L. Kovarik and S. C. Jacobson, *Anal. Chem.*, 2009, **81**, 7133–7140.

3 P. Abgrall and N. T. Nguyen, *Anal. Chem.*, 2008, **80**, 2326–2341.

4 M. Napoli, J. C. T. Eijkel and S. Pennathur, *Lab Chip*, 2010, **10**, 957–985.

5 L. Bocquet and P. Tabeling, *Lab Chip*, , DOI:10.1039/c4lc00325j.

6 R. B. Schoch, J. Han and P. Renaud, *Rev. Mod. Phys.*, 2008, **80**, 839–883.

7 E. A. Strychalski, H. W. Lau and L. A. Archer, *J. Appl. Phys.*, 2009, **106**, 024915.

8 M. Bassu, P. Holik, S. Schmitz, S. Steltenkamp and T. P. Burg, *Lab Chip*, 2016, **16**, 4546–4553.

9 S. Pennathur and J. G. Santiago, *Anal. Chem.*, 2005, **77**, 6782–6789.

10 Z. D. Harms, K. B. Mogensen, P. S. Nunes, K. Zhou, B. W. Hildenbrand, I. Mitra, Z. Tan,

A. Zlotnick, J. Org, P. Kutter and S. C. Jacobson, *Anal. Chem*, 2011, **83**, 9573–9578.

11 J. Wang, J. Hou, H. Zhang, Y. Tian and L. Jiang, *ACS Appl. Mater. Interfaces*, 2018, **10**, 2033–2039.

12 Z. Sun, T. Liao, Y. Zhang, J. Shu, H. Zhang and G.-J. Zhang, *Biosens. Bioelectron.*, 2016, **86**, 194–201.

13 C. Chen, Y. Li, S. Kerman, P. Neutens, K. Willems, S. Cornelissen, L. Lagae, T. Stakenborg and P. Van Dorpe, *Nat. Commun.*, 2018, **9**, 1733.

14 L. D. Menard and J. M. Ramsey, *Anal Chem*, 2013, **85**, 1146–1153.

15 W. Reisner, J. P. Beech, N. B. Larsen, H. Flyvbjerg, A. Kristensen and J. O. Tegenfeldt, *Phys. Rev. Lett.*, 2007, **99**, 058302.

16 G. F. Schneider, S. W. Kowalczyk, V. E. Calado, G. Pandraud, H. W. Zandbergen, L. M. K. Vandersypen and C. Dekker, *Nano Lett.*, 2010, **10**, 3163–3167.

17 X. Liang and S. Y. Chou, *Nano Lett.*, 2008, **8**, 1472–1476.

18 T. Tsukahara, W. Mizutani, K. Mawatari and T. Kitamori, *J. Phys. Chem. B*, 2009, **113**, 10808–10816.

19 C. Duan, W. Wang and Q. Xie, *Biomicrofluidics*, 2013, **7**, 026501.

20 D. Mijatovic, J. C. T. Eijkel and A. Van Den Berg, *Lab Chip*, 2005, **5**, 492–500.

21 D. G. Haywood, A. Saha-Shah, L. A. Baker and S. C. Jacobson, *Anal. Chem.*, 2015, **87**, 172–187.

22 Y. Xu, *Adv. Mater.*, 2018, **30**, 1–17.

23 D. Xia, J. Yan and S. Hou, *Small*, 2012, **8**, 2787–2801.

24 S. R. Leslie, A. P. Fields and A. E. Cohen, *Anal. Chem.*, 2010, **82**, 6224–6229.

25 J. S. Leith, A. Kamanzi, D. Sean, D. Berard, A. C. Guthrie, C. M. J. Mcfaul, G. W. Slater, H. W. De Haan and S. R. Leslie, *Macromolecules*, 2016, **49**, 9266–9271.

26 M. J. Ahamed, S. Mahshid, D. J. Berard, F. O. Michaud, R. Sladek, W. W. Reisner and S. R. Leslie, *Macromolecules*, 2016, **49**, 2853–2859.

27 A. Arsenault, J. S. Leith, G. Henkin, C. M. J. Mcfaul, M. Tarling, R. Talbot, D. Berard, F. Michaud, S. Scott and S. R. Leslie, *Rev. Sci. Instrum.*, 2015, **86**, 033701.

28 C. Zhou, T. Segal-Peretz, M. E. Oruc, H. S. Suh, G. Wu and P. F. Nealey, *Adv. Funct. Mater.*, 2017, **27**, 1701756.

29 P. Stroeve, M. Rahman, L. D. Naidu, G. Chu, M. Mahmoudi, P. Ramirez and S. Mafe, *Phys. Chem. Chem. Phys*, 2014, **16**, 21570.

30 D. Magde, W. W. Webb, E. Elson, M. Eigen, R. Rigler, U. Bertocci, C. Gabrielli, F. Huet, M. Keddam and P. Rousseau, *Proc. Natl. Acad. Sci. U. S. A*, 1972, **29**, 8203–8212.

31 S. L. Bocquet, P. Tabeling and L. Bocquet, *Lab Chip*, 2014, **14**, 3143–3158.

32 N. F. Durand, C. Dellagiacoma, R. Goetschmann, A. Bertsch, I. Mä rki, T. Lasser and P. Renaud, *Anal. Chem.*, 2009, **81**, 5407–5412.

33 S. J. De Carvalho, R. Metzler and A. G. Cherstvy, *Soft Matter*, 2015, **11**, 4430–4443.

34 M. Born and E. Wolf, *Principles of Optics*, Pergamon, Oxford, U.K., 6th edn., 1980.

35 D. F. Kienle and T. L. Kuhl, *Anal. Chem.*, 2014, **86**, 11860–11867.

36 J. Israelachvili, *Intermolecular and Surface Forces*, Elsevier, San Diego, 3rd edn., 2011.

37 K. D. Moller, in *Optics: Learning by Computing with Examples Using MathCAD*, Springer, New York, 2003, pp. 77–125.

38 G. B. Airy, *London, Edinburgh, Dublin Philos. Mag. J. Sci. 2.7*, 1833, 20–33.

39 S. Mahshid, M. J. Ahamed, D. Berard, S. Amin, R. Sladek, S. R. Leslie and W. W. Reisner, *Lab Chip*, 2015, **15**, 3013.

40 D. Berard, C. M. J. Mcfaul, J. S. Leith, A. K. J. Arsenault and F. Michaud, *Rev. Sci. Instrum*, 2013, **84**, 103704.

41 D. J. Berard, F. Michaud, S. Mahshid, M. J. Ahamed, C. M. J. Mcfaul, J. S. Leith, P. Bérubé, R. Sladek, W. Reisner and S. R. Leslie, *PNAS*, 2014, **111**, 13295–13300.

42 A. Plecis, R. B. Schoch and P. Renaud, *Nano Lett.*, 2005, **5**, 1147–1155.

43 S. Scott, Z. Ming Xu, F. Kouzine, D. J. Berard, C. Shaheen, B. Gravel, L. Saunders, A. Hofkirchner, C. Leroux, J. Laurin, D. Levens, C. J. Benham and S. R. Leslie, *Nucleic Acids Res.*, 2018, **46**, 4622–4631.

44 C. M. J. McFaul, J. Leith, B. Jia, F. Michaud, A. Arsenault, A. Martin, D. Berard and S. Leslie, in *Proc. SPIE 8811, Physical Chemistry of Interfaces and Nanomaterials XII*, 2013, p. 881102.

45 A. G. Cherstvy, *Biopolymers*, 2012, **97**, 311–317.

46 K. Ando, M. Tanabe and K. Morigaki, *Langmuir*, 2016, **32**, 7958–7964.